De-Embedding for Coupled Three-Port Devices

Yuandong Guo¹, Bo Pu², DongHyun Kim³, and Jun Fan⁴

Electromagnetic Compatibility Laboratory Missouri University of Science and Technology Rolla, Missouri, USA ¹ydggdd, ²bpdbh, ³dkim, ⁴jfan@mst.edu

Abstract—In many applications, the device under test (DUT) is embedded into a test setup. Various de-embedding techniques have been proposed to expose the real electrical behaviors of a DUT, e.g., the traditional thru-reflect-line and short-open-loadthru algorithms, where the T-matrix and its inverse form are adopted in the mathematical process. In the fields of radiofrequency and electromagnetic compatibility, a DUT may have three coupled ports, and the symmetry in the associated Smatrix breaks down, because the numbers of entry and exist ports are not equal, which results in a non-square T-matrix based upon the definitions. Given that the inverse expression of a nonsquare matrix does not exist, the conventional de-embedding methods are not applicable for a coupled three-port network. In this paper, a de-embedding algorithm which is feasible for coupled three-port devices is proposed and verified through the measurement-based studies. The de-embedding technique may also be applied on devices with more than three ports.

Keywords—coupling; de-embedding; S-parameter; T-matrix; test fixture; three-phase motor; AC bus bar.

I. INTRODUCTION

In many radiofrequency and electromagnetic compatibility scenarios, a multi-port device under test (DUT) is embedded into a test setup. In order to characterize the electrical performances of the DUT, de-embedding is generally needed during the post-processing phase.

The traditional de-embedding techniques [1][2] employ the T-matrix and its inverse form of both the DUT and test fixture. A network with even number of ports is symmetric, since it has the same number of entrance and exit ports. However, this symmetry may break down for networks with odd number of ports. In this case, their T-matrices are not square, and the inverse matrices do not exist [3]. Therefore, the conventional de-embedding techniques, e.g., thru-reflection-line [1], short-open-load-thru [2], and 2X-Thru algorithms [4][5], are only feasible for networks with even number of ports.

In this paper, we present a de-embedding approach, which can be applied to coupled three-port devices. This paper extends the application of the de-embedding algorithm documented in [6] by illustrating the mathematical derivations and measurement-based validation. The proposed technique can be further developed and applied to generic devices with odd number of ports, which will be reported in future publications.

The de-embedding method for one-port devices is briefly

explained in Section II, which is extended for the deembedding of uncoupled and coupled three-port devices in Section III and IV, respectively. The proposed de-embedding algorithm is verified through the measurement-based studies performed on a vehicular three-phase braking system and given in Section V. Section VI concludes this paper.

II. DE-EMBEDDING FOR ONE-PORT DEVICES

A. A Two-Port Network and Its S-matrix

Given a common two-port network shown in Fig. 1, the relationship between the incident waves a_i and reflected waves b_i are correlated in the S-matrix expressed by

$$\begin{pmatrix} b_1 \\ b_2 \end{pmatrix} = \begin{pmatrix} S_{11} & S_{12} \\ S_{21} & S_{22} \end{pmatrix} \begin{pmatrix} a_1 \\ a_2 \end{pmatrix}$$
 (1)

Expanding the matrices in (1) yields

$$b_1 = S_{11}a_1 + S_{12}a_2 \tag{2a}$$

$$b_2 = S_{21}a_1 + S_{22}a_2 \tag{2b}$$

Solving for a_2 and b_2 gives

$$a_2 = -\left[S_{21}\right]^{-1} \cdot S_{11} \cdot a_1 + \left[S_{21}\right]^{-1} \cdot b_1 \tag{3a}$$

$$b_2 = \left(S_{12} - S_{22} \cdot (S_{21})^{-1} \cdot S_{11}\right) \cdot a_1 + S_{22} \cdot (S_{21})^{-1} \cdot b_1 \tag{3b}$$

B. De-Embedding for One-Port Devices

Assuming a one-port network illustrated in Fig. 2, the "Total" is outlined by the dashed box, and the corresponding S-matrix, in which both a_1 and b_1 are included, is measurable. If the "Fixture" can be characterized through its S-matrix, the incident and reflected waves of the DUT, namely, b_2 and a_2 , can be obtained through (3), since

$$b_2 = a_{DUT} \tag{4a}$$

$$a_2 = b_{DUT} \tag{4b}$$

The S-parameter of the one-port DUT is: $S_{DUT} = \frac{b_{DUT}}{a_{DUT}} = \frac{a_2}{b_2}.$

III. DE-EMBEDDING FOR UNCOUPLED THREE-PORT DEVICES

For the uncoupled three-port network sketched in Fig. 3,

This work is supported in part by the National Science Foundation under Grant No. IIP-1916535.



Fig. 1. A representation of common two-port networks with incident and reflected waves.

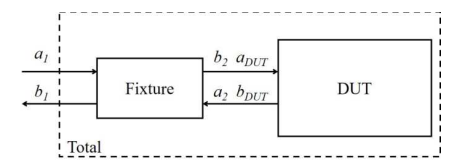


Fig. 2. A one-port device with both DUT and "Fixture" exhibited

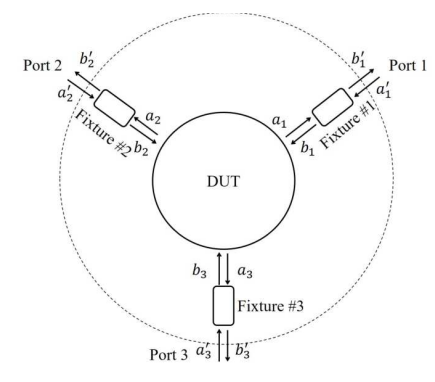


Fig. 3. An uncoupled three-port network. The dashed circle mimics the boundary of the "Total" structure, whose S-matrix can be acquired through measurements.

the unprimed coefficients, a_i and b_i , denote the incident and reflected waves of each fixture at the port adjacent to the DUT, respectively. The primed parameters, a_i and b_i , represent the incident and reflected waves at the measurable ports of the Total structure, whose boundary is mimicked by the dashed circle in Fig. 3.

It is evident that Fixture i, where i = 1, 2, 3, is a two-port network. Similar to (3a) and (3b), a_i and b_i can be readily depicted by a_i ' and b_i ' after expanding the associated S-matrix [6]:

$$a_{i} = -[S_{i,i}]^{-1} \cdot S_{i,i} \cdot a_{i}' + [S_{i,i}]^{-1} \cdot b_{i}' = A \cdot a_{i}' + B \cdot b_{i}'$$
 (5a)

$$b_{i} = (S_{ii} - S_{ii} \cdot (S_{ii})^{-1} \cdot S_{ii}) \cdot a_{i}' + S_{ii} \cdot (S_{ii})^{-1} \cdot b_{i}' = C \cdot a_{i}' + D \cdot b_{i}'$$
 (5b)

Since the three ports are uncoupled, the matrices A, B, C, and D only contain diagonal coefficients. The S-matrix of the DUT is derived as

$$S_{DUT} = \frac{\left[b_{DUT}\right]}{\left[a_{DUT}\right]} = \left(\left[A\right] + \left[B\right] \cdot \left[S'\right]\right) \cdot \left(\left[C\right] + \left[D\right] \cdot \left[S'\right]\right)^{-1} \tag{6}$$

where, S' is the S-matrix of total and available through measurements.

IV. DE-EMBEDDING FOR COUPLED THREE-PORT DEVICES

The general S-matrix expression manifesting the physical relationship between the incident and reflected waves for the coupled three-port device exhibited in Fig. 4 contains a 6×6

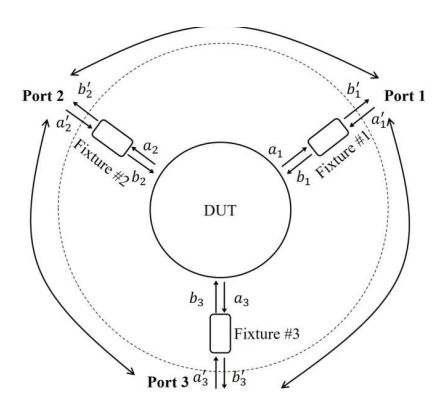


Fig. 4. A coupled three-port network

matrix, where the couplings are indicated by the non-diagonal elements as suggested in (7).

$$\begin{bmatrix} b_{1} \\ b_{1} \\ b_{2} \\ b_{2} \\ b_{3} \\ b_{3} \end{bmatrix} = \begin{bmatrix} S_{11} & S_{11} & S_{12} & S_{12} & S_{13} & S_{13} \\ S_{11} & S_{11} & S_{12} & S_{12} & S_{13} & S_{13} \\ S_{21} & S_{21} & S_{22} & S_{22} & S_{23} & S_{23} \\ S_{21} & S_{21} & S_{22} & S_{22} & S_{23} & S_{23} \\ S_{31} & S_{31} & S_{32} & S_{32} & S_{33} & S_{33} \\ S_{31} & S_{31} & S_{32} & S_{32} & S_{33} & S_{33} \end{bmatrix} \begin{bmatrix} a_{1} \\ a_{1} \\ a_{2} \\ a_{2} \\ a_{3} \\ a_{3} \end{bmatrix}$$

$$(7)$$

Re-writing the S-matrix in (7) with six equations and solving for the unprimed parameters, a_i and b_i , where i = 1, 2, 3, yields

$$a_1 = X_1b_1' + X_2b_2' + X_3b_3' + Y_1a_1' + Y_2a_2' + Y_3a_3'$$
 (8a)

$$a_2 = W_1b_1' + W_2b_2' + W_3b_3' + U_1a_1' + U_2a_2' + U_3a_3'$$
 (8b)

$$a_3 = J_1b_1' + J_2b_2' + J_3b_3' + K_1a_1' + K_2a_2' + K_3a_3'$$
 (8c)

$$b_{1} = (S_{11}X_{1} + S_{12}W_{1} + S_{13}J_{1})b_{1}' + (S_{11}X_{2} + S_{12}W_{2} + S_{13}J_{2})b_{2}'$$

$$+ (S_{11}X_{3} + S_{12}W_{3} + S_{13}J_{3})b_{3}' + (S_{11}' + S_{11}Y_{1} + S_{12}U_{1} + S_{13}K_{1})a_{1}'$$

$$+ (S_{12}' + S_{11}Y_{2} + S_{12}U_{2} + S_{13}K_{2})a_{2}' + (S_{13}' + S_{11}Y_{3} + S_{12}U_{3} + S_{13}K_{3})a_{3}'$$
(8d)

$$b_{2} = (S_{21}X_{1} + S_{22}W_{1} + S_{23}J_{1})b_{1}' + (S_{21}X_{2} + S_{22}W_{2} + S_{23}J_{2})b_{2}' + (S_{21}X_{3} + S_{22}W_{3} + S_{23}J_{3})b_{3}' + (S_{21}' + S_{21}Y_{1} + S_{22}U_{1} + S_{23}K_{1})a_{1}' + (S_{22}' + S_{21}Y_{2} + S_{22}U_{2} + S_{23}K_{2})a_{2}' + (S_{22}' + S_{21}Y_{3} + S_{22}U_{3} + S_{23}K_{3})a_{3}'$$
(8e)

$$b_{2} = (S_{31}X_{1} + S_{32}W_{1} + S_{33}J_{1})b_{1}^{'} + (S_{31}X_{2} + S_{32}W_{2} + S_{33}J_{2})b_{2}^{'}$$

$$+(S_{31}X_{3} + S_{32}W_{3} + S_{33}J_{3})b_{3}^{'} + (S_{31}Y_{1} + S_{32}U_{1} + S_{33}K_{1})a_{1}^{'}$$

$$+(S_{32}Y_{1} + S_{31}Y_{2} + S_{32}U_{2} + S_{33}K_{2})a_{2}^{'} + (S_{33}Y_{1} + S_{31}Y_{3} + S_{32}U_{3} + S_{33}X_{3})a_{3}^{'}$$

$$(8f)$$

where the mathematical expressions of the coefficients X_i , Y_i , W_i , U_i , J_i , and K_i , where i = 1, 2, 3, are given in the Appendix.

Equations (8a) \sim (8f) can be manifested in the matrix form shown as

$$\begin{bmatrix} b_{1} \\ b_{2} \\ b_{3} \\ a_{1} \\ a_{2} \\ a_{3} \end{bmatrix} = \begin{bmatrix} M_{11} & M_{12} & M_{13} & M_{14} & M_{15} & M_{16} \\ M_{21} & M_{22} & M_{23} & M_{24} & M_{25} & M_{26} \\ M_{31} & M_{32} & M_{33} & M_{34} & M_{35} & M_{36} \\ M_{41} & M_{42} & M_{43} & M_{44} & M_{45} & M_{46} \\ M_{51} & M_{52} & M_{53} & M_{54} & M_{55} & M_{56} \\ M_{61} & M_{62} & M_{63} & M_{64} & M_{65} & M_{66} \end{bmatrix} \begin{bmatrix} a_{1} \\ a_{2} \\ a_{3} \\ b_{1} \\ b_{2} \\ b_{3} \end{bmatrix}$$

$$(9)$$

where the elements in the matrix [M] can be readily identified. For the sake of simplicity, equation (9) can also be written as

$$\begin{bmatrix} b_{1} \\ b_{2} \\ b_{3} \\ a_{1} \\ a_{2} \\ a_{3} \end{bmatrix} = \begin{bmatrix} M_{D} & M_{C} \\ M_{B} & M_{A} \end{bmatrix} \begin{bmatrix} a_{1}^{'} \\ a_{2}^{'} \\ a_{3}^{'} \\ b_{1}^{'} \\ b_{2}^{'} \\ b_{3}^{'} \end{bmatrix}$$
(10)

The sub-matrices M_A , M_B , M_C , and M_D are suggested by the dashed lines in (9).

Assuming the total structure is characterized by [S'], the S-matrix of the DUT is determined through

$$[S_{DUT}] = ([M_A] + [M_B][S']) \cdot ([M_C] + [M_D][S'])^{-1}$$
 (11)

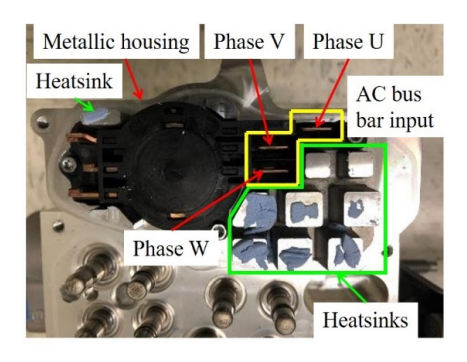
V. MEASUREMENT-BASED VALIDATION

The device is a three-phase permanent magnet synchronous motor (PMSM), which is utilized in a highly integrated vehicular braking system [7], whose top view is demonstrated in Fig. 5(a). Three ports are defined between each phase and PMSM's metallic housing for the VNA measurements, and the resulting S-matrix is adopted to reproduce the electrical characteristics in the frequency range of 100 kHz to 120 MHz. The accurate SPICE model of the PMSM is constructed with the three-phase AC bus bar incorporated, and the methodology is documented in [8].

In the 3D model illustrated in Fig. 5(b), where the multilayer printed circuit board (PCB) is about 1 mm above the AC bus bar but omitted in the figure due to confidentiality reasons, the parasitic capacitances from PCB nets and heatsinks to each bus bar are estimated in ANSYS Q3D [9]. It is found that the AC bus bar is tightly coupled to the PCB and heatsinks in the frequency range of interest, which means it has to be utilized in the full-wave simulation model together with the PCB and deembedded from the measured PMSM's S-matrix for the electromagnetic interference study.

The AC bus bar is cut at the junction point with the three-phase motor, and Fig. 6 shows the definitions of each port and the measurement configurations. The measurement is conducted using Agilent E5071C network analyzer. The Smatrix of the three-phase motor is also measured, which is regarded as the baseline data.

With the proposed de-embedding approach implemented, the good agreements shown in Fig. 7 verify the algorithm.



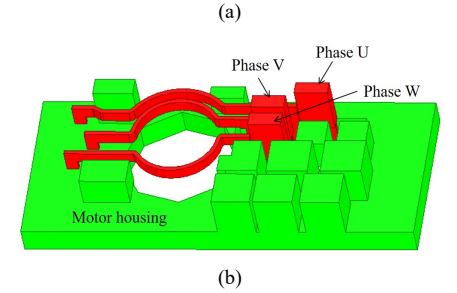


Fig. 5. (a) The top view of the PMSM under study, (b) the associated 3D model

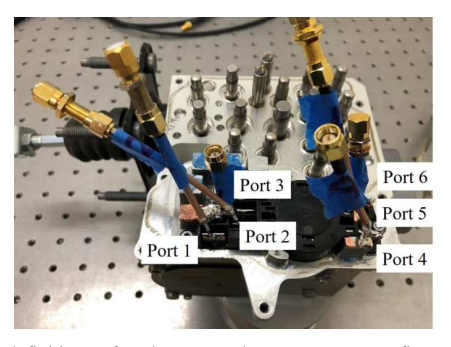


Fig. 6. The definitions of each ports and measurement configurations for the AC bus bar.

VI. CONCLUSION

With the limitations of using T-matrix for de-embedding explained, a de-embedding methodology suitable for coupled three-port devices is presented in this paper, which is developed based upon fundamental S-parameter concept and verified through a measurement-based case. The proposed deembedding algorithm can be further expanded for generic devices, which will be reported and verified in future publications.

APPENDIX

The expressions of the coefficients X_i , Y_i , W_i , U_i , J_i , and K_i , where i = 1, 2, 3, are given as

$$X_{1} = \frac{S_{23}S_{32} - S_{33}S_{22}}{S_{32}(S_{23}S_{11} - S_{13}S_{21}) + S_{12}(S_{33}S_{21} - S_{23}S_{31}) + S_{22}(S_{13}S_{31} - S_{33}S_{11})} \quad A.1$$

$$X_{2} = \frac{S_{33}S_{12} - S_{13}S_{32}}{S_{32}(S_{23}S_{11} - S_{13}S_{21}) + S_{12}(S_{33}S_{21} - S_{23}S_{31}) + S_{22}(S_{13}S_{31} - S_{33}S_{11})} \quad A.2$$

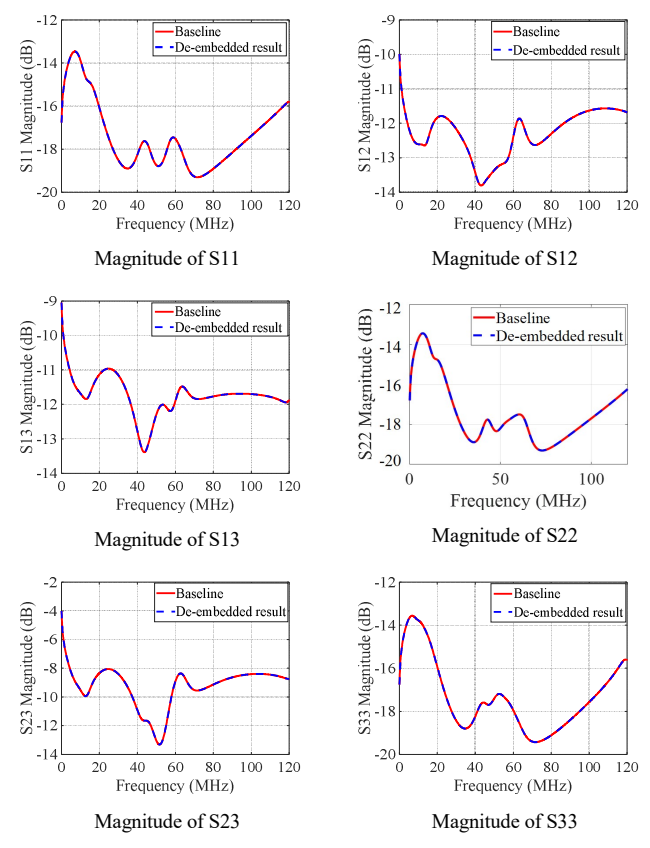


Fig. 7. The comparisons between the de-embedded and baseline data, which verify the proposed de-embedding approach.

$$\begin{split} X_3 &= \frac{S_{13}S_{22} - S_{23}S_{12}}{S_{32}(S_{23}S_{11} - S_{13}S_{21}) + S_{12}(S_{33}S_{21} - S_{23}S_{31}) + S_{22}(S_{13}S_{31} - S_{33}S_{11})} \qquad \text{A.3} \\ Y_1 &= \frac{S_{12}(S_{23}S_{31} - S_{33}S_{21}) + S_{32}(S_{13}S_{21} - S_{23}S_{11}) + S_{22}(S_{13}S_{31} - S_{33}S_{11})}{S_{32}(S_{23}S_{11} - S_{13}S_{21}) + S_{12}(S_{33}S_{21} - S_{23}S_{11}) + S_{22}(S_{13}S_{31} - S_{33}S_{11})} \qquad \text{A.4} \\ Y_2 &= \frac{S_{12}(S_{23}S_{32} - S_{33}S_{22}) + S_{32}(S_{13}S_{22} - S_{23}S_{12}) + S_{22}(S_{13}S_{31} - S_{33}S_{11})}{S_{32}(S_{23}S_{11} - S_{13}S_{21}) + S_{12}(S_{33}S_{21} - S_{23}S_{31}) + S_{22}(S_{13}S_{31} - S_{33}S_{11})} \qquad \text{A.5} \\ Y_3 &= \frac{S_{12}(S_{23}S_{33} - S_{33}S_{22}) + S_{32}(S_{13}S_{23} - S_{23}S_{13}) + S_{22}(S_{13}S_{31} - S_{33}S_{11})}{S_{32}(S_{23}S_{11} - S_{13}S_{21}) + S_{12}(S_{33}S_{21} - S_{23}S_{31}) + S_{22}(S_{13}S_{31} - S_{33}S_{11})} \qquad \text{A.6} \\ W_1 &= \frac{S_{23}S_{31} - S_{33}S_{21}}{S_{32}(S_{23}S_{11} - S_{13}S_{21}) + S_{12}(S_{33}S_{21} - S_{23}S_{31}) + S_{22}(S_{13}S_{31} - S_{33}S_{11})} \qquad \text{A.7} \\ W_2 &= \frac{S_{13}S_{31} - S_{33}S_{21}}{S_{32}(S_{23}S_{11} - S_{13}S_{21}) + S_{12}(S_{33}S_{21} - S_{23}S_{31}) + S_{22}(S_{13}S_{31} - S_{33}S_{11})} \qquad \text{A.8} \\ W_3 &= \frac{S_{23}S_{11} - S_{13}S_{21}}{S_{32}(S_{23}S_{11} - S_{13}S_{21}) + S_{12}(S_{33}S_{21} - S_{23}S_{31}) + S_{22}(S_{13}S_{31} - S_{33}S_{11})} \qquad \text{A.9} \\ \end{array}$$

 $U_{1} = \frac{S_{11}(S_{33}S_{21} - S_{23}S_{31}) + S_{31}(S_{23}S_{11} - S_{13}S_{21}) + S_{21}(S_{13}S_{31} - S_{21}S_{11})}{S_{23}(S_{23}S_{11} - S_{13}S_{21}) + S_{22}(S_{13}S_{31} - S_{21}S_{11})}$

$$U_{2} = \frac{S_{11}(S_{33}S_{22} - S_{23}S_{32}) + S_{31}(S_{23}S_{12} - S_{13}S_{22}) + S_{21}(S_{13}S_{32} - S_{21}S_{12})}{S_{12}(S_{23}S_{11} - S_{13}S_{21}) + S_{22}(S_{13}S_{21} - S_{23}S_{11})} - A.11$$

$$U_{3} = \frac{S_{11}(S_{33}S_{23} - S_{23}S_{33}) + S_{31}(S_{23}S_{13} - S_{13}S_{23}) + S_{21}(S_{13}S_{33} - S_{21}S_{13})}{S_{32}(S_{23}S_{11} - S_{13}S_{21}) + S_{12}(S_{33}S_{21} - S_{23}S_{31}) + S_{22}(S_{13}S_{31} - S_{33}S_{11})} \quad \text{A.12}$$

$$J_{1} = \frac{S_{22}S_{31} - S_{32}S_{21}}{S_{22}(S_{22}S_{11} - S_{12}S_{21}) + S_{12}(S_{22}S_{21} - S_{22}S_{21}) + S_{22}(S_{12}S_{21} - S_{22}S_{11})}$$
 A.13

$$J_2 = \frac{S_{32}S_{11} - S_{31}S_{12}}{S_{32}(S_{23}S_{11} - S_{13}S_{21}) + S_{12}(S_{33}S_{21} - S_{23}S_{31}) + S_{22}(S_{13}S_{31} - S_{33}S_{11})}$$
 A.14

$$J_{3} = \frac{S_{21}S_{12} - S_{11}S_{22}}{S_{32}(S_{32}S_{11} - S_{12}S_{21}) + S_{12}(S_{32}S_{21} - S_{22}S_{21}) + S_{22}(S_{12}S_{21} - S_{22}S_{11})}$$
 A.15

$$K_{1} = \frac{S_{12}(S_{31}S_{21} - S_{21}S_{31}) + S_{32}(S_{21}S_{11} - S_{11}S_{21}) + S_{22}(S_{11}S_{31} - S_{31}S_{11})}{S_{32}(S_{23}S_{11} - S_{13}S_{21}) + S_{12}(S_{33}S_{21} - S_{23}S_{31}) + S_{22}(S_{13}S_{31} - S_{33}S_{11})}$$
 A.16

$$K_{2} = \frac{S_{12}(S_{31}S_{22} - S_{21}S_{31}) + S_{32}(S_{21}S_{12} - S_{11}S_{21}) + S_{22}(S_{11}S_{32} - S_{31}S_{12})}{S_{32}(S_{23}S_{11} - S_{13}S_{21}) + S_{12}(S_{33}S_{21} - S_{23}S_{31}) + S_{22}(S_{13}S_{31} - S_{33}S_{11})}$$
 A.17

$$K_{3} = \frac{S_{12}(S_{31}S_{23} - S_{21}S_{33}) + S_{32}(S_{21}S_{13} - S_{11}S_{23}) + S_{22}(S_{11}S_{33} - S_{31}S_{13})}{S_{32}(S_{23}S_{11} - S_{13}S_{21}) + S_{12}(S_{33}S_{21} - S_{23}S_{31}) + S_{22}(S_{13}S_{33} - S_{31}S_{11})}$$
 A.18

REFERENCES

- [1] L. Ye et al., "Thru-Reflect-Line Calibration Technique: Error Analysis for Characteristic Impedance Variations in the Line Standards," in IEEE Transactions on Electromagnetic Compatibility, vol. 59, no. 3, pp. 779-788, June 2017.
- H. Cho and D. E. Burk, "A three-step method for the de-embedding of high-frequency S-parameter measurements," in IEEE Transactions on Electron Devices, vol. 38, no. 6, pp. 1371-1375, June 1991.
- J. Frei, X. -D. Cai and S. Muller, "Multiport \$S\$ -Parameter and \$T\$ -Parameter Conversion With Symmetry Extension," in IEEE Transactions on Microwave Theory and Techniques, vol. 56, no. 11, pp. 2493-2504, Nov. 2008.
- B. Chen et al., "Differential S-Parameter De-embedding for 8-Port Network," 2018 IEEE Symposium on Electromagnetic Compatibility, Signal Integrity and Power Integrity (EMC, SI & PI), 2018, pp. 52-56.
- B. Chen, J. He, Y. Guo, S. Pan, X. Ye and J. Fan, "Multi-Ports ([\$2^{n}\$) 2×-Thru De-Embedding: Theory, Validation, and Mode Conversion Characterization," in IEEE Transactions on Electromagnetic Compatibility, vol. 61, no. 4, pp. 1261-1270, Aug. 2019.
- B. Pu, J. Kim, and W. Nah, "A de-embedding technique of a three-port network with two ports coupled," in Journal of Electromagnetic Engineering and Science, vol. 15, no.4, pp. 258-265, Oct.2015.
- Y. Guo et al., "Ground Bridge Effect on Reduction of Conducted Emission from Three-Phase Motor Drive System," 2019 International Symposium on Electromagnetic Compatibility - EMC EUROPE, 2019, pp. 854-859.
- [8] Y. Guo et al., "High-Frequency Modeling of Permanent Magnet Synchronous Motor Considering Internal Imbalances," 2021 Asia-Pacific International Symposium on Electromagnetic Compatibility (APEMC), 2021, pp. 1-3.
- C. Che, H. Zhao, Y. Guo, J. Hu and H. Kim, "Investigation of Segmentation Method for Enhancing High Frequency Simulation Accuracy of Q3D Extractor," 2019 IEEE International Conference on Computational Electromagnetics (ICCEM), 2019, pp. 1-3.

A.9

A.10